

# Myocardial Blood Flow from Dynamic PET using Independent Component Analysis

Alexander Karpikov, Hemant Tagare, *Senior Member, IEEE*, Tim Mulnix, Jean-Dominique Gallezot, Albert Sinusas, Chi Liu, *Member, IEEE*, and Richard E. Carson, *Member, IEEE*

**Abstract**—Generation of parametric images of myocardial blood flow (MBF) from dynamic PET requires a reproducible and reliable method to obtain left and right ventricular time-activity curves. We propose the use of Independent Component Analysis (ICA) on PET temporal information to segment the image data into three categories: right ventricle (RV), left ventricle (LV) and myocardium. ICA is an established signal processing technique that assumes that the dynamic signal in each voxel is a linear mixture of signals from statistically independent sources. The mixing process is due to cardiac motion and partial volume effects. Due to its ability to find the intensity of the underlying sources, ICA generates a 3D map of the mixing coefficients that allows the segmentation of structures. Dynamic cardiac PET data were acquired with a Siemens Biograph mCT PET/CT scanner using Rb-82 and [<sup>15</sup>O]water in nonhuman primate and pigs with injections of different activities. The Dice similarity coefficient (DSC) was used to compare the segmentations between scans of different species with different tracers. The LV and RV regions were used to calculate input functions for kinetic analysis and MBF estimation.

Pairwise comparisons of the segmentations between different [<sup>15</sup>O]water PET scans gave DSC of  $0.91 \pm 0.09$  and  $0.92 \pm 0.08$  for the RV and LV segmentations, respectively. For Rb-82 PET scans, the DSC values were of  $0.89 \pm 0.09$  and  $0.85 \pm 0.10$  for RV and LV. We used contrast CT as a gold standard for the LV and RV segmentations. Pairwise comparisons of the segmentations between different contrast CT and Rb-82 PET scans gave DSC of  $0.86 \pm 0.09$  and  $0.85 \pm 0.09$  for the RV and LV, respectively. Our work shows the reliability and reproducibility of the results of the segmentation algorithm. High quality parametric images of MBF and the kinetic parameters were obtained. These results suggest that ICA may be useful to extract time-activity curves for kinetic MBF analysis. The effects of partial volume on input TAC determination were also evaluated.

## I. INTRODUCTION

PET imaging is an important tool for studying cardiac function including myocardial blood flow (MBF). The accuracy of MBF computation depends on the accuracy of the input time-activity curves (TACs) of the model. Accurate estimation of input curves requires careful segmentation of the left ventricle (LV) and right ventricle (RV). Segmentation of

cardiac PET data is challenging due to the higher noise level of PET data compared to CT or MRI. Independent Component Analysis (ICA) is an established technique in signal processing [1]. It has been successfully applied to the blind deconvolution problem, i.e., finding the independent signals from their mixtures without knowing the mixing coefficients. Dynamic cardiac PET data provide another example of a problem of mixed signals. Signals from blood in LV and RV plus the myocardium signal are mixed due to cardiac motion and the partial volume effect. In this work, we used ICA to segment the data in order to get reproducible and reliable RV and LV TACs for MBF analysis. ICA segments data using its temporal properties: the source corresponding to the RV is highest during the initial bolus passage through the RV. The LV source is active at a later stage when tracer enters the LV. The myocardium source has slower kinetics. For MBF calculations we used standard kinetic models [2,3] applied to nonhuman primate and pig PET data with Rb-82 and [<sup>15</sup>O]water.

## II. METHODS

### A. Data acquisition

Scans were performed on Biograph mCT TOF PET/CT scanner (Siemens Medical Solutions USA, Inc.). A rhesus monkey and two pigs were studied with [<sup>15</sup>O]water and Rb-82. Injections of different activities were used for this study. All the scans were in the resting state to permit assessment of reproducibility. Table I summarizes the information about the scans.

Table I. Scan description

Species	Tracers	# of injections (scans)	Contrast CT
Rhesus monkey	[ <sup>15</sup> O]water	5	no
Pig #1	Rb-82	3	no
Pig #2	Rb-82	3	yes
	[ <sup>15</sup> O]water	2	

PET data were acquired in list mode format and reconstructed using Siemens TrueX reconstruction algorithm, a 3D PSF ordinary-Poisson ordered-subset-expectation-maximization reconstruction algorithm [4] with TOF. Parameters for the reconstruction were 3 iterations and 21 subsets with 2x2x2 mm voxels. The frame duration for the dynamic PET reconstruction was 3s. The time interval

Manuscript received November 13, 2012. This work was supported by a research contract from Siemens Medical Solutions.

Alexander Karpikov, Tim Mulnix, Jean-Dominique Gallezot, Chi Liu, and Richard E. Carson are with the PET center, Yale University, New Haven, CT 06520 USA

Hemant Tagare is with Departments of Diagnostic Radiology and Biomedical Engineering, Yale University, New Haven, CT 06511 USA

Albert Sinusas is with Departments of Internal Medicine and Diagnostic Radiology, Yale University, New Haven, CT 06520 USA

between adjacent frames was 1s, i.e., with overlapping frames to increase temporal sampling. Contrast CT scan was acquired for Fig #2.

### B. ICA Algorithm

For a dataset with  $m$  voxels and  $n$  time points, consider a linear mixture of  $k$  independent components (here  $k=3$ ), which can be written as a matrix product:

$$\mathbf{x} = \mathbf{A}\mathbf{s} \quad (1)$$

where  $\mathbf{x}$  is the  $m \times n$  data matrix, each row corresponding to a time point of a particular voxel.  $\mathbf{s}$  is a  $k \times n$  matrix, with each row being a source vector corresponding to the TAC of each component.  $\mathbf{A}$  is the mixing matrix ( $m \times k$ ) which has only spatial dependency (See Fig. 1). ICA considers the distribution of the radioactivity values (ignoring their order) and assumes that components are statistically independent and have non-Gaussian distribution. This assumption allows ICA to estimate  $\mathbf{A}$  as well as  $\mathbf{s}$ . For further theoretical discussions of ICA as well as different numerical implementation, please refer to [1]. We used Fast ICA [5], an algorithm based on a fixed-point iteration scheme maximizing non-Gaussianity (skewness) of the distribution of the source vectors as a measure of statistical independence. As a standard step of Fast ICA data pre-processing (whitening) the dimensionality of the data was reduced by applying PCA and keeping only first seven PCA eigenvalues.

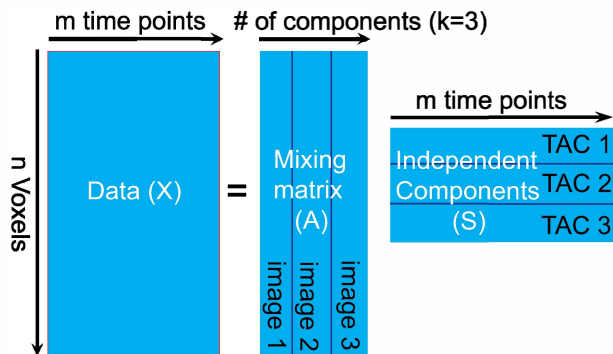


Fig. 1. Schematic representation of ICA algorithm.

## III. ANALYSIS

### A. ICA

Fast ICA was applied to the [ $^{15}\text{O}$ ]water and Rb-82 cardiac PET data. The number of independent components was chosen to be three (RV, LV, and myocardium).

The Dice similarity coefficient (DSC) [6] was used to compare the consistency of the segmentations across scans of different injections:

$$DSC = 2 \frac{B \cap Y}{B + Y} \quad (2)$$

where B (blue) and Y (yellow) are two segmentations represented by their voxel locations,  $\cap$  is the intersection of two regions and  $+$  is the sum of two regions (Fig. 2). DSC takes values between zero and one and is equal to one for two identical segmentations.

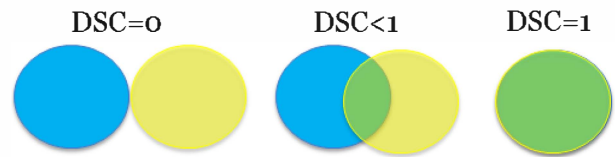


Fig. 2. Schematic depiction of Dice similarity coefficient (DSC).

### B. Parametric image model

The 4-parameter kinetic model for Rb-82 data was applied pixel-by-pixel with the LV input function and 2 spill-in terms [2]:

$$C_T(t) = K_1 * C_A(t) \otimes \exp(-k_2 * t) + V_A C_A(t) + V_{RV} C_{RV}(t) \quad (3)$$

where  $C_T$  is the tissue activity,  $K_1$  is the myocardium inflow,  $k_2$  is the myocardial tissue egress (outflow), and  $C_A(t)$  and  $C_{RV}(t)$  are the arterial (LV) and RV TACs, respectively. An example of  $C_A(t)$  and  $C_{RV}(t)$  curves is shown in Fig. 3. A similar 4-parameter kinetic model is used for [ $^{15}\text{O}$ ]water data [3]:

$$C_T(t) = MBF * PTF * C_A(t) * \exp\left(-MBF * \frac{t}{V_T}\right) + V_A C_A(t) + V_{RV} C_{RV}(t) \quad (4)$$

where  $V_T$  is volume of distribution or partition coefficient of water ( $V_T=0.91$ ), and PTF is the perfusable tissue fraction.

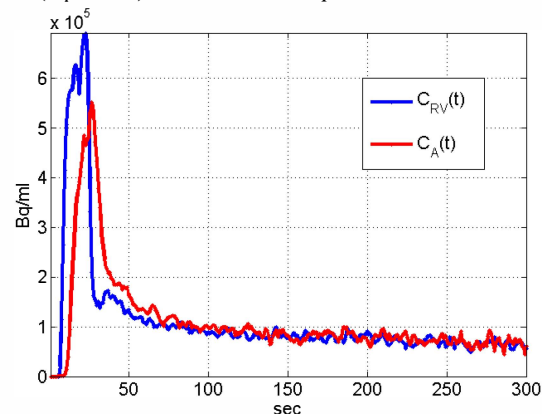


Fig. 3. An example of  $C_A(t)$  and  $C_{RV}(t)$  curves estimated from ICA-derived regions from a pig study

Both  $C_A(t)$  and  $C_{RV}(t)$  curves have highly non-Gaussian distribution functions. This is demonstrated by the long-tailed histogram of  $C_{RV}(t)$  shown in Fig. 4. ICA was thus expected to be an effective algorithm for defining LV and RV regions, since it finds independent components by maximizing non-Gaussianity of each source.

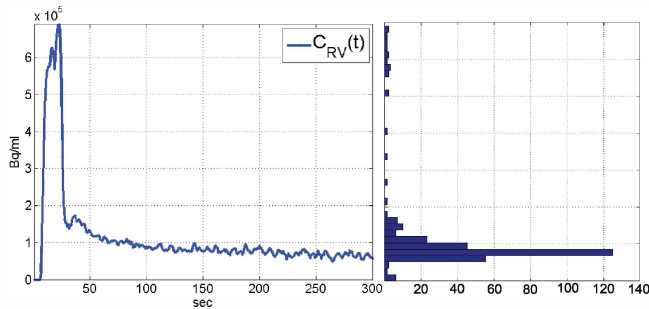


Fig. 4. An example of  $C_{RV}(t)$  curve (left panel) and its histogram (right panel) showing a non-Gaussian distribution.

ICA gives the mixing matrix  $A$  ( $m \times 3$ ) as its output. The three components correspond to RV, LV or myocardium as shown in Fig. 5. By identifying the component corresponding to the LV and choosing only pixels with component scores above a certain threshold, we obtain the mask region to derive the LV input curve. The same procedure is applied for the RV curve. The thresholds were chosen in consistent way such that the volumes for RL and VL are the same for across the runs. This is used to compare the consistency of the segmentations. The numerical value of the thresholds was chosen based on the visual assessment of the shape of the regions and input curves derived from those regions.

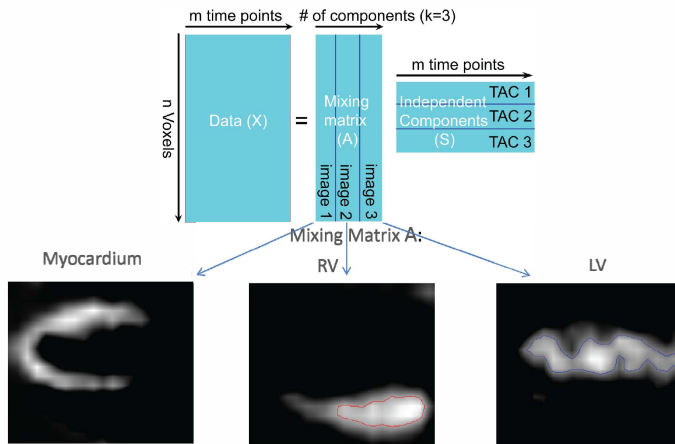


Fig. 5. Application of ICA for RV and LV segmentation. Images on the bottom are the ICA-derived component maps

A basis function implementation of weighted least squares minimization was used to fit the voxel TACs to the kinetic models. Noise equivalent counts (NEC) were used as weights. The model produces parametric images of  $V_{RV}$ ,  $V_A$ ,  $PTF$  and  $MBF$ .

We investigated the influence of the partial volume effect on the kinetic model parameters. Specifically, the simulation concerned the bias in the LV and RV curves measured in the vicinity of the myocardium, since the partial volume effects of

the myocardial region are included in the kinetic model. Mathematically, this idea can be expressed as:

$$C_A(t) = \alpha C_{A \text{ true}}(t) + (1-\alpha) C_m(t) \quad (5)$$

where the measured arterial input function  $C_A(t)$  is contaminated by spill-in from the myocardium, i.e., the measurement is the linear combination of the true arterial function  $C_{A \text{ true}}$  and the myocardium signal  $C_m$ . The situation when  $\alpha=0$  corresponds to no partial volume effect (zero bias). Simulations were performed using experimentally measured input curves from Rb-82 and  $[^{15}\text{O}]$ water scans. These input curves were obtained by using a very stringent threshold for the ICA mixing matrix giving LV ROIs which suffer minimal partial volume effect.  $C_m$  was modeled using typical kinetic parameters for the myocardium. For a given value of  $\alpha$ , the biased LV curve was calculated with Eq. 5, the model fitting was applied, and the percent bias in the kinetic parameters was determined.

#### IV. RESULTS AND DISCUSSIONS

In these initial data, reliable segmentation of tissues with different TACs was achieved with ICA. Pairwise comparisons of the segmentations between different PET scans gave high values of DSC, as shown in Table II.

Table II. ICA segmentation comparison

Species	Tracers used	RV DSC between all pairs	LV DSC between all pairs
Rhesus monkey	$[^{15}\text{O}]$ water (5 scans)	$0.91 \pm 0.09$	$0.92 \pm 0.08$
Pig #1	Rb-82 (3 scans)	$0.89 \pm 0.09$	$0.84 \pm 0.10$
Pig #2	Rb-82 (2 scans) $[^{15}\text{O}]$ water (3 scans)	$0.88 \pm 0.09$	$0.86 \pm 0.10$

Fig. 6 shows examples of high quality parametric images of MBF, PTF,  $V_A$  and  $V_{RV}$  from  $[^{15}\text{O}]$ water in the rhesus monkey. Gaussian smoothing (FWHM= 3.5 mm) was applied to the data after the fitting. The numerical values of the resulting parametric images were consistent with the literature; for example, the peak values of LV and RV volume fractions were near 1.0. A more thorough quantitative evaluation of this approach is underway.

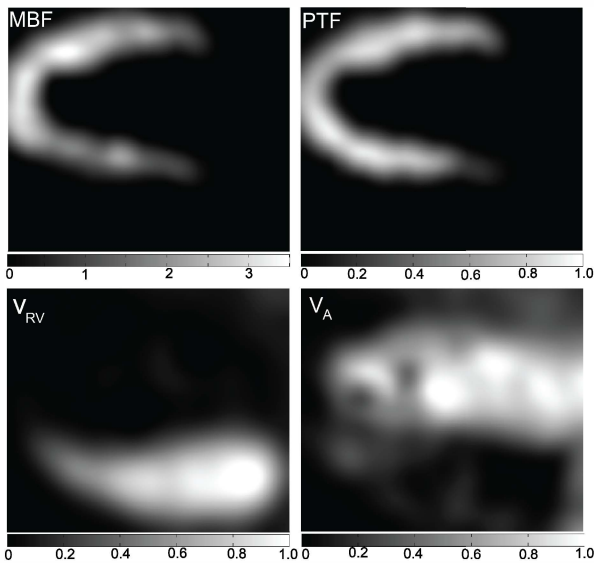


Fig. 6. Examples of parametric images from  $[^{15}\text{O}]$ water in the rhesus monkey. Top left: MBF (myocardial blood flow)  $[\text{ml}/(\text{min} \cdot \text{cm}^3)]$ . Top right: PTF (perfusible tissue fraction). Bottom left:  $V_{\text{RV}}$  (Right ventricle blood volume). Bottom right:  $V_{\text{A}}$  (Left ventricle arterial blood volume).  $V_{\text{A}}$  and  $V_{\text{RV}}$  are the spill-in coefficients for the myocardium. MBF and PTF images were filtered based on the myocardium segmentation obtained using ICA.

In one pig study, we used contrast CT as a gold standard for the LV and RV segmentations. See Fig. 7 for the comparison of contrast CT and  $[^{15}\text{O}]$ water scan. The thresholds for CT and PET segmentations were chosen in consistent way such that the volumes for RL and VL are the same across CT and PET segmentations. Pairwise comparisons of the segmentations between different contrast CT and Rb-82 PET scans gave DSC of  $0.86 \pm 0.09$  for the RV segmentations and  $0.85 \pm 0.09$  for the LV segmentations.

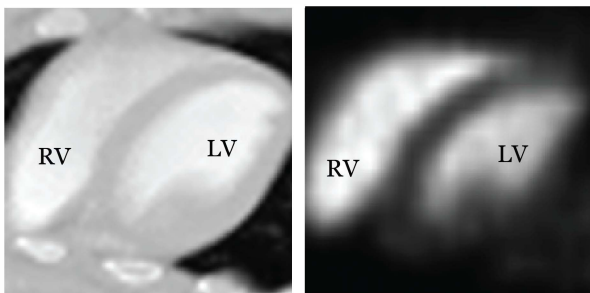


Fig. 7. Contrast CT for Pig #2 averaged over one cardiac cycle (left panel).  $[^{15}\text{O}]$ water scan for the same pig averaged over 40 sec after the injection (right panel).

An important step in this evaluation includes the optimization of thresholding of the LV and RV ICA-derived components to produce the respective TACs. Fig. 8 displays the change in the LV input curve corresponding to changes in ROI used to derive it. MBF clearly depends on the choice of the ROI used to derive the LV input function. Specifically, the use of LV input function derived from larger ROIs would bias the LV TAC, underestimating the activity at early times and possibly overestimating it at later times, if the myocardial activity exceeds that in the blood pool. Ultimately, MBF values using ICA-derived TACs will be assessed for test/retest

reliability and accuracy vs. arterial input function measurements.

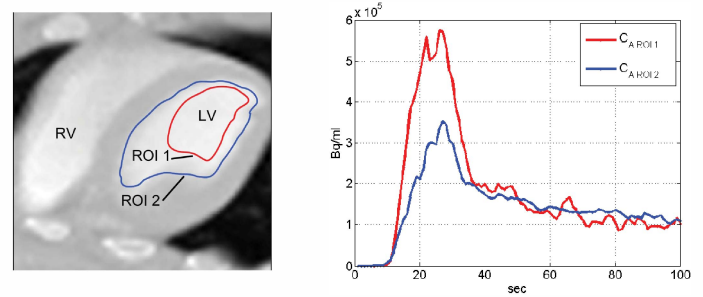


Fig. 8. Choice of ROI (Pig #2 data) for the  $C_{\text{A}}(t)$  input curve (left panel) and the corresponding input curves (right panel).

Fig. 9 shows the results of simulation studies for partial volume effect described by Eq. 5. The graph displays the bias introduced by partial volume effects. We can clearly see that the partial volume effect become more pronounced with increasing  $\alpha$ , i.e., increasing LV ROI size. Based on the substantial magnitude of these biases, careful selection of the region, i.e., careful selection of the ICA threshold, will be important for accurate kinetic parameter estimation.

## V. SUMMARY AND FUTURE WORK

Based on these initial data, our work demonstrates the reliability and reproducibility of segmenting LV and RV structures using ICA. Since this technique was used in 2 species and with 2 tracers, it suggests that ICA may be a highly robust approach to extract regions for voxel-by-voxel measurement of myocardial blood flow with PET. Our future work will include optimization of the thresholding procedure for RV and LV segmentation to control the partial volume effect. In addition, comparisons of Rb-82 and  $[^{15}\text{O}]$ water MBF measurements will be performed in animal and human studies. We will also validate MBF computations in animal scans with microspheres experiments.

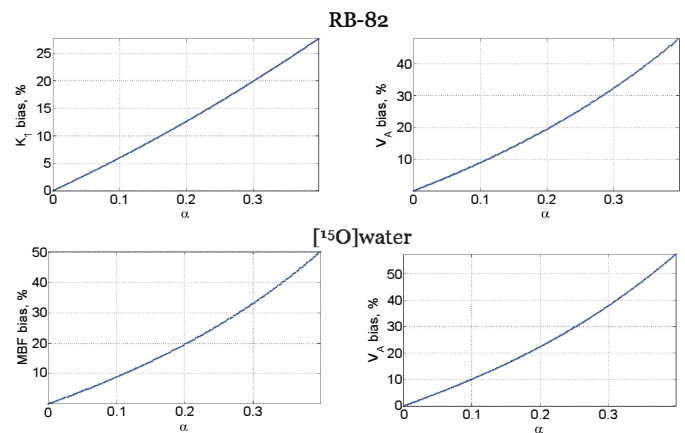


Fig. 9. Kinetic coefficients bias due to the partial volume effect in the LV region for Rb-82 (top) and  $[^{15}\text{O}]$ water (bottom). The term  $\alpha$  defines the magnitude of the partial volume effect.

#### ACKNOWLEDGMENT

We thank Zhongdong Sun for programming support and the staff of the Yale PET Center for the studies that formed the basis of this work. This work was sponsored by a grant from Siemens Medical Systems.

#### REFERENCES

- [1] A. Hyvarinen, J. Karhunen, and E. Oja, *Independent component analysis*. New York: J. Wiley, 2001.
- [2] G. El Fakhri, A. Sitek, B. Guerin, M. F. Kijewski, M. F. Di Carli, and S. C. Moore, "Quantitative dynamic cardiac  $^{82}\text{Rb}$  PET using generalized factor and compartment analyses," *JNM*, vol. 46, pp 1264-1271, May 2005.
- [3] H. J. Harms, P. Knaapen, S. de Haan, R. Halbmeijer, A. A. Lammertsma, and M. Lubberink, "Automatic generation of absolute myocardial blood flow images using  $[\text{O}-15]\text{H}_2\text{O}$  and a clinical PET/CT scanner," *European Journal of Nuclear Medicine and Molecular Imaging*, vol. 38, pp. 930-939, May 2011.
- [4] V. Y. Panin, F. Kehren, C. Michel, and M. Casey, "Fully 3-D PET reconstruction with system matrix derived from point source measurements," *Ieee Transactions on Medical Imaging*, vol. 25, pp. 907-921, Jul 2006.
- [5] A. Hyvarinen, "Fast and robust fixed-point algorithms for independent component analysis," *Ieee Transactions on Neural Networks*, vol. 10, pp. 626-634, May 1999.
- [6] K. H. Zou, S. K. Warfield, A. Bharatha, C. M. C. Tempany, M. R. Kaus, S. J. Haker, W. M. Wells, F. A. Jolesz, and R. Kikinis, "Statistical validation of image segmentation quality based on a spatial overlap index - Scientific reports," *Academic Radiology*, vol. 11, pp. 178-189, Feb 2004.